JOURNAL OF COMPUTATIONAL PHYSICS 5, 103–124 (1970)

A Lagrangian Method for Calculating the Dynamics of an Incompressible Fluid with Free Surface*

C. W. HIRT, J. L. COOK, AND T. D. BUTLER

Los Alamos Scientific Laboratory, University of California, Los Alamos, New Mexico 87544

Received June 9, 1969

A new method is presented for the numerical solution of the transient flow of viscous incompressible fluids having free surfaces. The method is based on Lagrangian coordinates in contrast to other methods, which use the Eulerian representation. Lagrangian coordinates permit the accurate treatment of fluid interfaces and free surfaces, and make it a simple matter to include the effects of surface tension. Several examples illustrate the properties of this new technique.

A. INTRODUCTION

Many methods have been developed for calculating the transient dynamics of incompressible fluids. A partial list of developers is given in [1] and [2]. All techniques in [1] use the vorticity and stream function as primary dependent variables. There are two advantages with this approach for two-dimensional problems. Only two dependent variables are needed, and mass is easily conserved, since the use of a stream function identically satisfies the mass conservation condition

$$\nabla \cdot \mathbf{u} = 0. \tag{1}$$

The disadvantages associated with the vorticity-stream function method are its extension to three dimensions, which requires the introduction of a vector potential for velocity [3], and the difficulty encountered in satisfying free surface boundary conditions. To overcome these difficulties the methods in [2] were developed using the pressure and velocity as primary dependent variables. These methods maintain accuracy with a minimum of computer time through the use of a corrective procedure [2, 4].

All methods in [1] and [2] are based on the Eulerian concept of a fluid moving through a stationary network of cells, and are most useful for problems involving large fluid distortions. Their biggest drawback is the lack of definition given fluid

* This work was performed under the auspices of the United States Atomic Energy Commission.

interfaces, small localized regions of the flow, and low amplitude motions. For example, to include surface tension forces complicated spline fitting techniques are needed to estimate surface curvature from a set of surface marker particles [5]. furthermore, interfaces between different fluid species can be handled only when density differences are small and the flow is of low viscosity [6].

To overcome the difficulties associated with free boundaries in Eulerian methods, this paper describes a new Lagrangian technique for incompressible fluids, called LINC. The fluid is covered by a mesh of cells whose vertices move with the fluid. In this way, fluid in the interior of a cell always remains in that cell, and fluid boundaries always move with the cell boundaries. Although the Lagrangian method is not applicable to flows undergoing large distortions, where cells can be twisted into unacceptable shapes, its advantages are the ease with which it handles free surfaces and interfaces, which makes it applicable to a wide variety of problems.

As it is presented here, the LINC method is applicable to two-dimensional flows in plane Cartesian coordinates, but it can be extended to three-dimensional flows and other types of coordinate systems.

In an incompressible Lagrangian calculation the volume of each mesh cell must remain constant during the course of a calculation. To satisfy this constraint LINC uses a corrective procedure as described in Section B. Boundary conditions are discussed in Section C, and the inclusion of surface tension is considered in Section D. The computational stability of the method is discussed in Section E. Section F presents sample calculations that include fluid sloshing in a rectangular tank, growth of a Rayleigh-Taylor instability, and the transient formation of a meniscus. Detailed difference equations are given in the Appendix, but are omitted from the main body of the paper to simplify presentation of the essential features of the LINC method.

B. Basic Methodology

The Eulerian equations of motion for an incompressible fluid are the Navier-Stokes equations

$$(\partial \mathbf{u}/\partial t) + \mathbf{u} \cdot \nabla \mathbf{u} = -\nabla \phi + \nabla \cdot \nu \mathbf{E} + \mathbf{g} \tag{2.a}$$

and the incompressibility condition

$$\nabla \cdot \mathbf{u} = 0. \tag{2.b}$$

Since the density ρ is constant we have introduced the kinematic pressure $\phi = p/\rho$ and the kinematic viscosity ν. The body force is denoted by $\mathbf{g}$, and $\mathbf{E}$ is the rate of strain tensor whose components are

$$E_{\alpha\beta} = (\partial u_\beta/\partial x_\alpha) + (\partial u_\alpha/\partial x_\beta). \tag{3}$$

The position vector for a fluid element, $\mathbf{r}$, satisfies the equation

$$d\mathbf{r}/dt = \mathbf{u}. \tag{4}$$

The left side of (2.a) is the total convective derivative of $\mathbf{u}$, which represents the time rate of change of $\mathbf{u}$ in a fluid element moving with the fluid. Thus, it is the time rate of change for a Lagrangian fluid element. Although the derivatives on the right side of (2.a) could be written in terms of the Lagrangian coordinates, it is more convenient to retain them in their Eulerian form. Therefore, the Lagrangian equations we wish to solve are the momentum equation

$$d\mathbf{u}/dt = -\nabla\phi + \nabla \cdot \nu\mathbf{E} + \mathbf{g}, \tag{5.a}$$

and the position equation

$$d\mathbf{r}/dt = \mathbf{u}. \tag{5.b}$$

The incompressibility condition (2.b) is replaced by the constraint that the volume of each fluid element remain constant.

The numerical solution of (5) is accomplished by introducing finite difference approximations for the derivatives in these equations. For a two-dimensional calculation, the fluid is subdivided into a set of quadrilateral cells whose vertices are labeled by indices i and j as shown in Fig. 1. For each vertex there is stored a position, $\mathbf{r} = (x_i^j, y_i^j)$, and velocity, $\mathbf{u} = (u_i^j, v_i^j)$. Pressures are stored for the center of each cell, e.g., $\phi_{i+1/2}^{j+1/2}$ is the pressure for the cell shown in Fig. 1. Volumes (areas in two-dimensions) are also stored for each cell.

The quantities stored for the cells and their vertices are advanced in time through a sequence of small time steps, δt. The necessary steps in completing one cycle of

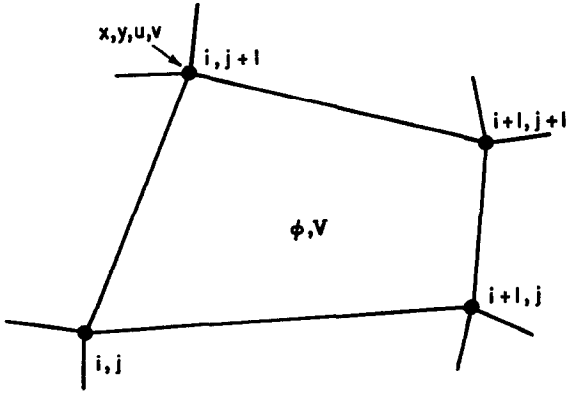

FIG. 1. Cell layout with i, j indices.

time advancement consist of first determining the pressure in each cell under the constraint that each cell will have the same volume after advancement as it had before advancement. Then new values of $\mathbf{u}$ are calculated, and finally, the vertices are moved to new positions.

Let ${}^{n}u_i{}^{j}$ denote the value of u at vertex (i, j) at time $n\,\delta t$ and similarly for the other variables. Then the finite difference approximation used for (5.b) is

$$ {}^{n+1}\mathbf{r}_i{}^{j} = {}^{n}\mathbf{r}_i{}^{j} + \delta t\, {}^{n+1}\mathbf{u}_i{}^{j}. \tag{6} $$

An approximation for ${}^{n+1}\mathbf{u}_i{}^{j}$ can be derived by averaging each term in (5.a) over twice the volume associated with each vertex. A vertex volume will be defined as the average volume of the cells surrounding the vertex, hence, it remains constant in time. Since the left side of (5.a) is the convective derivative of $\mathbf{u}$, the time derivative operator can be taken outside the volume integral,

$$ \frac{1}{V}\frac{d}{dt}\int_V \mathbf{u}\, dV \approx \frac{{}^{n+1}(V\mathbf{u})_i{}^{j} - {}^{n}(V\mathbf{u})_i{}^{j}}{V\delta t}. $$

Because V is constant in time this can be simplified to

$$ \frac{1}{V}\frac{d}{dt}\int_V \mathbf{u}\, dV \approx \frac{{}^{n+1}\mathbf{u}_i{}^{j} - {}^{n}\mathbf{u}_i{}^{j}}{\delta t}. \tag{7} $$

The right side of (5.a) is easily approximated too. The volume integral reduces to a surface integral (or line integral in two dimensions),

$$ \frac{1}{V}\int_V (-\nabla\phi + \nabla\cdot\nu\mathbf{E})\, dV = \frac{1}{V}\int_S (-\mathbf{n}\phi + \nu\mathbf{n}\cdot\mathbf{E})\, dS, \tag{8} $$

where $\mathbf{n}$ is the unit outward normal to the surface S.

In the difference approximations for the right side of (8) presented in the Appendix, the line integral is taken around the dashed contour shown in Fig. (2). This contour encloses a volume that is not equal to twice the vertex volume when the cells deviate from parallelograms. The reason for using twice the vertex volume as a factor in these difference approximations, instead of the actual integration volume, is to achieve rigorous conservation of momentum. This choice assures that the forces across each integration surface are equal and opposite, which is not the case if the actual integration volume is used. In addition, the ratio of twice the vertex volume to the actual integration volume reduces to unity with vanishing mesh sizes so that the difference equations are consistent approximations to the differential equations as they stand.

While the particular difference approximations presented in the Appendix are relatively simple, other difference approximations could be devised. However, the

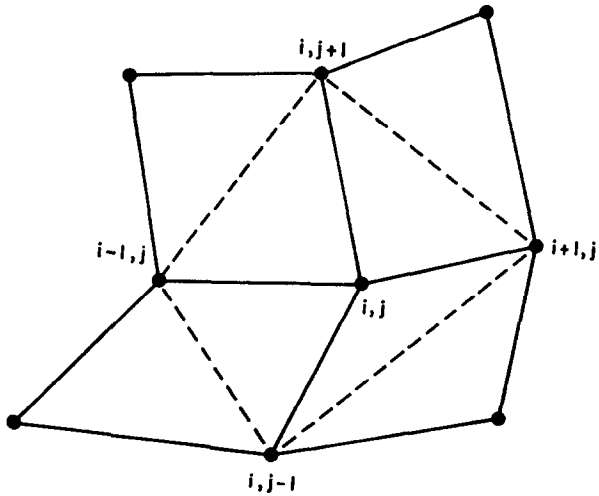

FIG. 2. Dashed lines outline area about i, j vertex for taking averages used in momentum equations.

basic LINC method is independent of this choice. Thus, for purposes of illustration, it is only necessary to write

$$^{n+1}\mathbf{u}_i^j = {}^n\mathbf{u}_i^j + \delta t\, \mathbf{A}_i^j, \tag{9}$$

where $\mathbf{A}_i^j$ is the net acceleration on vertex (i, j), and it may be calculated by any conservative difference method.

In an incompressible fluid the volume of each Lagrangian cell must remain constant. The area of a quadrilateral at time step $n + 1$, whose vertices are at positions (x_k, y_k) with $k = 1, 2, 3, 4$ labeled counterclockwise, is

$$^{n+1}V = \sum_{k,\ell} a_{k\ell}^{n+1} x_\ell^{n+1} y_k, \tag{10}$$

where $a_{k\ell}$ is the matrix

$$a_{k\ell} = 1/2 \begin{pmatrix} 0 & -1 & 0 & 1 \\ 1 & 0 & -1 & 0 \\ 0 & 1 & 0 & -1 \\ -1 & 0 & 1 & 0 \end{pmatrix}. \tag{11}$$

The accelerations that determine new vertex positions are not arbitrary, but must leave all cell volumes (10) unchanged. In the exact differential equations this condition requires the pressure to satisfy a certain Poisson equation. In the finite difference approach the necessary pressure equation is derived by inserting (9) into

(6) and the result into (10). The outcome, which is to be considered as an equation for the pressure, is

$$
\begin{aligned}
{}^{n+1}V = \sum_{\ell,\ell} a_{\ell\ell}\{&x_\ell y_\ell + \delta t(u_\ell y_\ell + x_\ell v_\ell) \\
&+ \delta t^2(u_\ell v_\ell + A_{x_\ell} y_\ell + x_\ell A_{y_\ell}) \\
&+ \delta t^3(A_{x_\ell} v_\ell + u_\ell A_{y_\ell}) + \delta t^4 A_{x_\ell} A_{y_\ell}\}.
\end{aligned} \tag{12}
$$

All positions and velocities on the right side of (12) are evaluated at time level n, so the pressures are the only unknowns. Equation (12) is an approximation to the Taylor series expansion for the volume,

$${}^{n+1}V = {}^nV + \delta t\,{}^n\left(\frac{\partial V}{\partial t}\right) + \delta t^2\,{}^n\left(\frac{\partial^2 V}{\partial t^2}\right) + \text{partial}\left\{\delta t^3\,{}^n\left(\frac{\partial^3 V}{\partial t^3}\right) + \delta t^4\,{}^n\left(\frac{\partial^4 V}{\partial t^4}\right)\right\}. \tag{13}$$

The last two terms are not complete, since terms of order δt^2 were neglected in (9). These partial terms are of higher order and are dropped from further consideration. Also, a coefficient of 1/2 does not appear in the δt^2 term because vertices are moved with velocities at time $(n + 1)\,\delta t$ rather than $(n + 1/2)\,\delta t$. Moving vertices with the average velocity $1/2({}^n\mathbf{u} + {}^{n+1}\mathbf{u})$ would introduce a factor of 1/2, but in the first test program this would have required the storage of two velocity values and was not considered worthwhile.

The constancy of cell volumes implies that ${}^{n+1}V = {}^0V$, and consequently, that the δt and δt^2 coefficients in (12) individually vanish. Closer investigation reveals that the δt coefficient is a finite difference approximation for the volume integral of $\nabla \cdot \mathbf{u}$, which should be zero. When the δt^2 coefficient is set to zero the result is an approximation for the usual Poisson equation for pressure,

$$\nabla^2\phi + \nabla \cdot (\mathbf{u} \cdot \nabla\mathbf{u}) = 0. \tag{14}$$

Actually the δt^2 coefficient also contains terms proportional to the divergence of the viscous and gravitational accelerations. Although these terms vanish in differential form, they do not vanish in finite difference form for a nonrectangular mesh.

By finding pressures that satisfy (12), when all other quantities are known at time level n and with ${}^{n+1}V$ set equal to the initial cell volume, it is clear that we always maintain constant cell volumes.

In attempting to solve (12) for ϕ, it is tempting to drop the zero-th order term $({}^0V - {}^nV)$ and the δt terms, and simply set the δt^2 term equal to zero. We do not do this, however, since the lower order terms serve as corrective elements that allow a coarse solution to be used while still maintaining accurate volume conservation

[4]. For example, if an error is made in solving (12) and ${}^{n}V$ is too small, the term $({}^{0}V - {}^{n}V)$ acts as a positive source that drives the pressure up and forces the volume to increase back to its initial value.

Many iteration schemes are available for solving the pressure equations. We use a Gauss-Seidel technique, in which successive sweeps are made through the mesh to advance the pressure values and new values are used for subsequent calculations as they become available. A successive over-relaxation process has also proven useful on occasion. The complete pressure equation is detailed in the Appendix.

This completes the necessary difference equations. A complete cycle of calculation consists of first solving the pressure equation (12), then calculating new velocities from (9), and finally, moving vertices to new positions using (6). If the pressures are determined to an accuracy of ϵ, new cell volumes will differ from their initial values by an amount proportional to ϵ, and $\nabla \cdot \mathbf{u}$ will differ from zero by a similar amount. The corrective procedure prevents these errors from accumulating after many calculational cycles.

C. Boundary Conditions

Three types of boundary conditions are considered: rigid walls, free surfaces, and material interfaces. At a rigid boundary, such as the bounding wall of a container, fluid may slip freely along the wall or it may stick to it. A free-slip condition is used if the viscosity of the fluid is so low that it produces a boundary layer thinner than the local finite cell thickness, or if the boundary is to represent a plane of symmetry. A no-slip condition is used for viscous flows with well defined boundary layers.

We shall first describe the general treatment of rigid boundary conditions, and then give a more convenient method for free-slip walls. At a rigid wall the normal velocity is zero and the tangential velocity may or may not be zero. In either case, substitution of (6) into (10) must take into account these known velocities. The pressure equation for a boundary cell will be similar to (12) except that the appropriate wall velocities and their accelerations must be set to zero. This prescription is applicable along any boundary composed of straight line segments. Of course, additional considerations are needed for free slip walls if vertices are to slide over bends in the boundary. In the case of a straight free-slip wall, the tangential velocity is calculated by averaging the momentum equation over the area enclosed by the dashed contour shown in Fig. 3. A viscous stress along the wall is determined from the condition that the normal derivative of the tangential velocity is zero, or equivalently, the vorticity is zero at the wall.

This treatment of rigid boundaries implies that (12) has a different form for boundary and interior cells, making its solution by computer somewhat com-

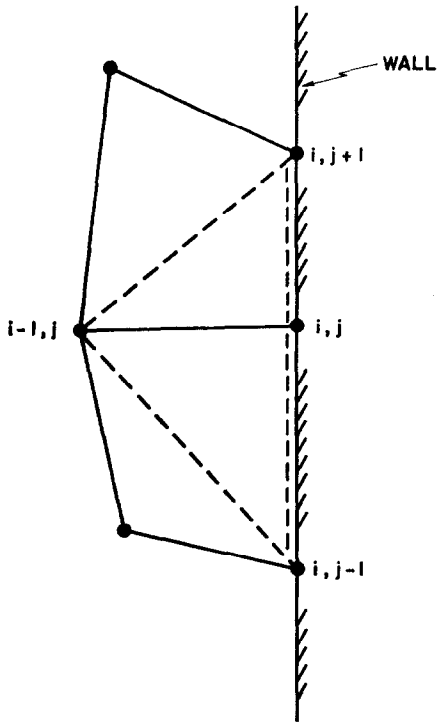

FIG. 3. Dashed lines outline integration area about a free-slip wall vertex.

plicated. For a free-slip wall this complication can be eliminated by using cells outside the wall and then treating wall vertices as interior vertices. Cells are constructed outside the wall by reflecting the cells inside, and pressures in the outside cells are chosen to make the normal acceleration at the wall equal to zero. A pressure outside is directly related to the pressure in its symmetric neighbor, provided a special volume ratio is inserted in the body acceleration term for vertices on walls normal to this acceleration, and a corresponding source term is inserted in pressure equations (see Appendix). The pressure used in a cell outside a right vertical wall at $i = I$ is

$$\phi_{I+1/2}^{j+1/2} = \phi_{I-1/2}^{j+1/2} + \frac{g_x}{2}(x_I^{j+1} - x_{I-1}^{j} + x_I^{j} - x_{I-1}^{j+1}). \tag{15}$$

The pressure used in a cell below a bottom horizontal wall at $j = J$ is

$$\phi_{i+1/2}^{J-1/2} = \phi_{i+1/2}^{J+1/2} - \frac{g_y}{2}(y_{i+1}^{J+1} - y_i^{J} + y_i^{J+1} - y_{i+1}^{J}). \tag{16}$$

For curved or slanted walls it is better to use the general approach and not employ outside cells. The rigid boundaries used in the sample calculations of Section F are free-slip boundaries, and the calculations take advantage of the simplified approach.

Material boundaries are treated somewhat differently. The average stress on a vertex at an interface is obtained by integrating around two half contours; one lying entirely within one material and the other lying in the other material, as in Fig. 4. The contours coincide along the interface, but are traversed in different

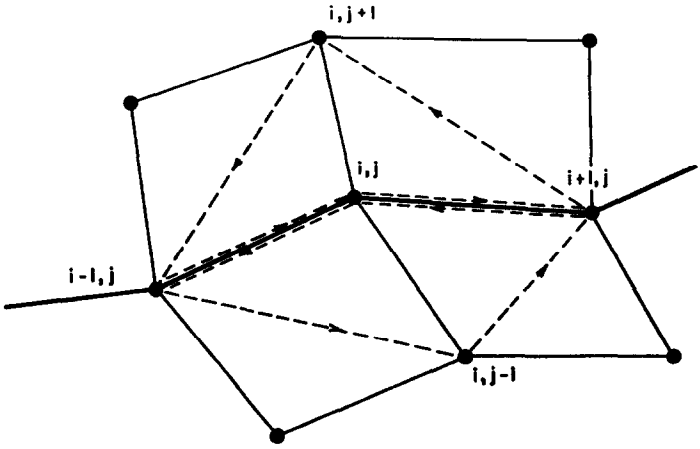

FIG. 4. Dashed lines outline integration paths used at a material interface. Heavy line indicates material interface.

directions. The boundary condition at an interface is the continuity of the stress tensor,

$$\Omega = -\phi \mathbf{I} + \nu \mathbf{E}, \tag{17}$$

where $\mathbf{I}$ is the identity tensor. Therefore, the integrations along the interface cancel and the resultant path of integration is the edge of the quadrilateral centered at the vertex.

At a free surface with unit outward normal $\mathbf{n}$, the boundary condition is

$$\Omega \cdot \mathbf{n} = 0. \tag{18}$$

To satisfy this condition it is tempting to treat surface vertices like free-slip wall vertices and integrate the stress over a partial integration area that lies entirely within the fluid. Because of (18), when the integration is transformed to a surface integral no contribution is received from integrating along the surface. Unfortunately there is a flaw in this approach. The average acceleration obtained in this way

should be associated with a vertex located at the center of the integration area. If the velocity tangent to the surface is varying in the normal direction, then assigning the calculated velocity to the surface vertex is incorrect. A similar error is not committed at a free-slip wall, because there the normal derivative of the tangential velocity is zero.

Since the acceleration of surface vertices cannot be calculated using partial integration areas, we have used the alternate method of inserting extra cells outside the surface. Take, for example, a free surface extending along $j = J$. Cells are constructed above the surface by extending the line segment connecting $(i, J-1)$ to (i, J) out to a distance equal to its length. The end of this extension defines the new vertex $(i, J+1)$. The construction is repeated for each i, and connecting vertices at $j = J+1$ completes the construction. Pressures in these cells are chosen to give the correct applied pressure, ϕ^{app}, at the surface,

$$\phi_{i+1/2}^{J+1/2} = 2(\phi^{\text{app}})_{i+1/2}^{J} - \phi_{i+1/2}^{J-1/2}. \tag{19}$$

Viscous stresses, if small, can still be integrated along the surface as a first approximation. For very viscous flows, however, it is important to correctly satisfy the free surface stress conditions [7]. One possibility is to extrapolate the acceleration calculated for the center of the partial integration area at the surface out to the surface edge. Of course this must be done in a way that preserves the volume of surface cells, but it should present no exceptional difficulties.

D. Surface Tension

The inclusion of surface tension forces in the LINC method is relatively easy compared with Eulerian methods. Consider a surface at $j = J$ on which there is surface tension σ. The surface tension force on a surface vertex (i, J) is the vector sum of a force of magnitude σ directed toward the right vertex $(i+1, J)$ and a force of magnitude σ directed toward the left vertex $(i-1, J)$,

$$\begin{aligned}\mathbf{F}_i^J = \mathbf{i}\left\{\frac{\sigma(x_{i+1}^J - x_i^J)}{r_R} + \frac{\sigma(x_{i-1}^J - x_i^J)}{r_L}\right\} \\ + \mathbf{j}\left\{\frac{\sigma(y_{i+1}^J - y_i^J)}{r_R} + \frac{\sigma(y_{i-1}^J - y_i^J)}{r_L}\right\},\end{aligned} \tag{20}$$

where $\mathbf{i}$ and $\mathbf{j}$ are unit vectors in the x and y directions, and

$$r_R = [(x_{i+1}^J - x_i^J)^2 + (y_{i+1}^J - y_i^J)^2]^{1/2},$$
$$r_L = [(x_i^J - x_{i-1}^J)^2 + (y_i^J - y_{i-1}^J)^2]^{1/2}.$$

If a vertex lies at the intersection of a free surface with a rigid wall it cannot have an acceleration normal to the wall, but adhesion will modify its tangential motion. Adhesion effects are included by adding a force on the corner vertex, directed along the wall and out of the surface, with magnitude $\gamma - \sigma$, where γ is a measure of the adhesion. When γ equals σ there is no attraction between the fluid and the wall. When γ exceeds σ the fluid wets the wall.

Equation (20) expresses the force on a surface vertex. To obtain the acceleration it must be remembered that surface vertices have only one half the mass assigned to interior vertices, and corner vertices have only one fourth the mass. The mass of a vertex is equal to its volume times the fluid density.

E. Computational Stability

A complete stability analysis of the LINC difference equations has not been made, but experience with simpler equations does give us a guide in outlining the limits of stability of this new method. In an analysis of one-dimensional Lagrangian difference equations, Fromm [8] has shown that the parabolic and hyperbolic portions of the equations can, for all practical purposes, be considered separately. Thus, if viscosity is present, there must be a limit imposed on the size of δt to prevent an instability of the type that occurs with simple diffusion equations,

$$\nu \delta t < \frac{\delta x^2 \, \delta y^2}{2(\delta x^2 + \delta y^2)}. \tag{21}$$

The space increments in a Lagrangian calculation vary in space and time so we must satisfy (21) in all regions of the flow for all time.

As for the hyperbolic portion of our equations, it is obvious that a vertex should not be moved so far that it crosses over a neighboring vertex. Thus, we require that

$$\delta t \left| \frac{(\mathbf{u}_a - \mathbf{u}_b) \cdot \delta \mathbf{r}}{\delta \mathbf{r} \cdot \delta \mathbf{r}} \right| < 1, \tag{22}$$

where $\delta \mathbf{r}$ is the vector distance from a vertex a, with velocity $\mathbf{u}_a$, to its neighbor vertex b, with velocity $\mathbf{u}_b$. Such a relation must hold for every pair of neighboring vertices in the mesh.

Another type of stability problem was encountered in the Marker-and-Cell (MAC) method. There the nonlinear convection terms in the Eulerian equations of motion gave rise to truncation errors that were diffusion-like terms with negative coefficients [9]. If these terms are not compensated for with a sufficiently large value of ν, a pure growing type of instability can occur. In the LINC method there are no explicit convection terms and this problem does not arise. Consequently, we

can perform calculations with the viscosity set equal to zero. This does not imply that such calculations actually correspond to infinite Reynolds numbers. There are diffusion-like truncation errors of order δt^2 arising from other sources, and these errors may obscure the effects of a very small viscosity.

Aside from errors arising in the approximation of the acceleration terms, all truncation errors are proportional to powers of δt, and can be easily controlled by keeping δt small. Thus, the only troublesome errors arise from approximations of the acceleration terms, which depend on the orientation and size of the Lagrangian zones. These errors are difficult to control since zones generally become more skewed as a calculation proceeds, and the introduction of more cells for better resolution increases the requirements for computer storage and computing time. We shall see effects of these errors in the examples of the next section.

When surface tension is considered, an additional stability condition must be imposed. If the surface vertices are displaced from an otherwise flat surface to form a sawtooth looking surface they experience a restoring force caused by the surface tension. Having too large a value of δt will over correct the surface configuration and produce an inverted sawtooth shape with larger amplitude. Repetition of such an over correction leads to an oscillating and exponentially growing surface instability. A simple analysis of the maximum δt that does not lead to an overshoot gives the stability condition,

$$\frac{4\sigma\,\delta t^2}{\rho V_0\,\delta x} \leqslant 1, \tag{23}$$

where σ is the surface tension coefficient, V_0 is the volume of the surface cells, and δx is their width.

F. Sample Applications

This new computing technique is best illustrated by discussing the results of several calculations. These include the sloshing of fluid in a rectangular tank, Rayleigh-Taylor instability, and the formation of a meniscus. A study of these examples shows the advantages and limitations of the LINC method.

In the first example, fluid initially at rest in a rectangular tank is impulsively set into oscillation by a cosine pressure pulse applied at the surface. A linear analysis for the change in surface elevation, η, above the initially undisturbed surface height D, gives

$$\eta = -A\sqrt{\frac{\xi}{gD}}\sin\left(t\sqrt{\frac{g\xi}{D}}\right)\cos kx, \tag{24}$$

where

$$\xi = kD \tanh(kD). \tag{25}$$

Here $k = 2\pi/\lambda$, where λ is the disturbance wave length, $g_y = -g$ is the acceleration of gravity, and the initial pressure pulse on the surface is described by

$$\phi = A\,\delta(t)\cos kx, \tag{26}$$

where $\delta(t)$ is the Dirac delta function.

Calculational results for this problem are shown in Fig. 5, where $g = 1.0$, $D = 15$, $\lambda = 80$, and $A = 11.78$. The Lagrangian mesh consisted of square cells, with 40 in the x direction and 15 in the y direction. The boundaries of the computing mesh are rigid free-slip walls representing planes of reflection. The calculation was performed with a viscosity of $\nu = 0.1$ to compare with a MAC calculation described in reference [10].

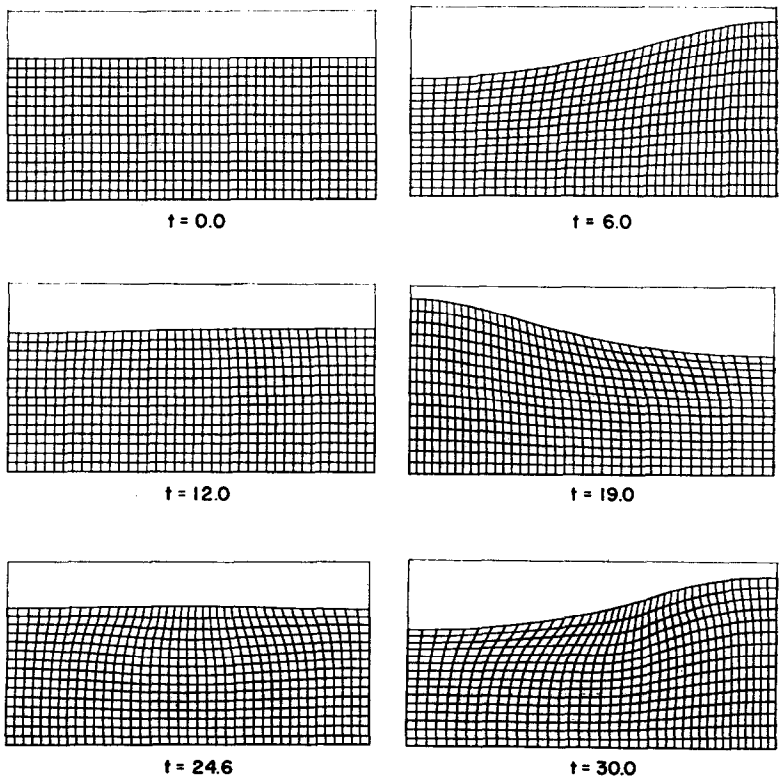

FIG. 5. Fluid configurations for a sloshing wave shown at the times indicated.

Figure 5 shows the fluid configuration at successive times during its evolution. The time increment between frames is approximately the theoretical quarter period of oscillation. The over-all configuration of the cells has changed in the one period of oscillation between the second and last frames. This change is a result of nonlinear effects, which introduce a disturbance of wavelength $\lambda/2$. Because of the distortion in cell shapes in the last frame, the surface curled up during the return slosh to the left, and the calculation had to be terminated.

Nonlinear effects influence the amplitude of the surface as indicated in Fig. 6. The elevated portion of the surface, the spike, has a larger amplitude than the linear theory would suggest, while the depressed portion of the surface, the bubble, has a smaller amplitude. Similar results were obtained with the MAC method developed by Harlow and Welch [10]. A direct comparison of the MAC and LINC methods is shown in Fig. 7. The irregularity of the surface in the MAC calculation is caused by the motion of the surface through the fixed rectangular cells. It has recently been shown by Chan [11] that these fluctuations can be considerably reduced by using more accurate velocity and pressure interpolations near the surface. The

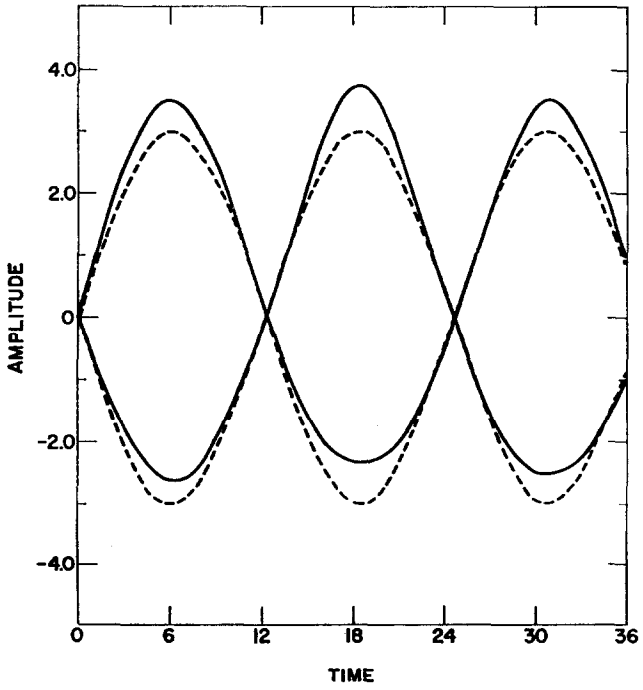

FIG. 6. Amplitude of spike and bubble (solid lines) versus time as compared with the linear theory (dashed lines).

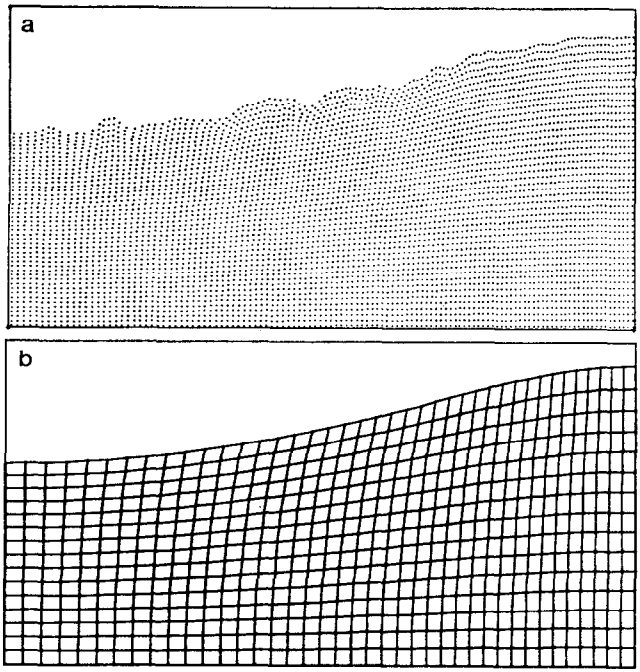

FIG. 7. Comparison of (a) MAC calculation and (b) LINC calculation for the sloshing wave at time 6.0.

LINC method always maintains a well defined surface. In general, the LINC method is most useful for problems not involving large distortions, but requiring an accurate knowledge of the dynamics of free surfaces and material interfaces.

While nonlinear effects have clearly affected the spike and bubble amplitudes, the oscillation frequency in this example was nearly equal to that predicted by the linear theory. This result was predicted by Tadjbakhsh and Keller [12]. Those authors have shown that the frequency of oscillation decreases with increasing amplitude if the initial depth of fluid is larger than 0.17λ. For smaller depths the frequency increases with increasing amplitude. In our example the depth is 0.1875λ, which is very near the neutral point where frequency is independent of amplitude.

As a second example we consider the development of a Rayleigh-Taylor instability. Reversing the direction of gravity in the previous example produces an unstable situation. When the surface is perturbed its amplitude continues to grow without oscillation. The example illustrated in Figs. 8–9 was chosen to duplicate the MAC calculation presented in reference [10]. The surface was perturbed with a pressure pulse of the form (26) with $A = 5.0$, $\lambda = 9.6$, $g_y = 1.0$, $\nu = 0.01$, and $d = 8.0$. The calculation employed 12 cells in the x direction and 20 cells in the

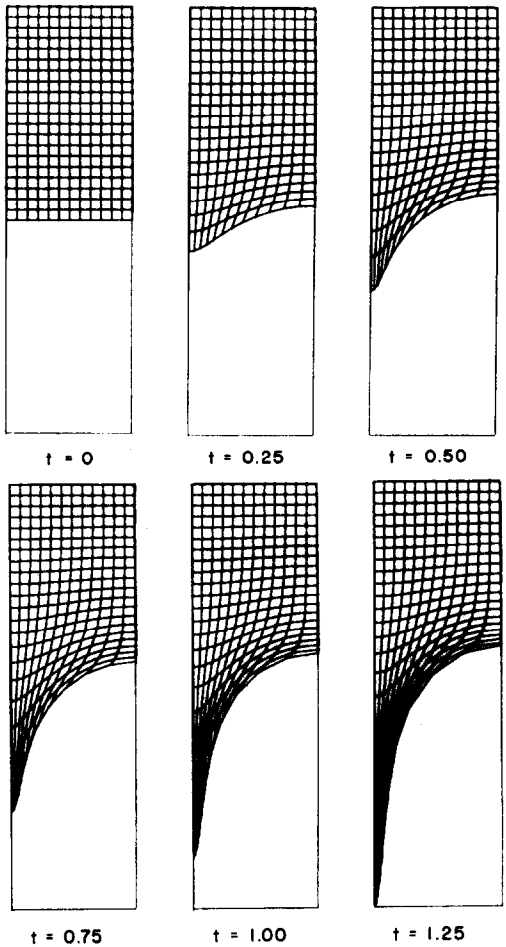

FIG. 8. Fluid configurations for a Rayleigh-Taylor instability shown at the times indicated.

y direction. The values of g and D for this problem may be considered as defining the problem units.

For times less than 0.7 problem units the calculational results are in excellent agreement with the MAC calculation. At late times the spike correctly grows with the constant acceleration of gravity, but the asymptotic bubble speed is somewhat

caused by the coarseness of the Lagrangian zones. The calculation was repeated with zones twice as big, and a linear extrapolation to zero zone size gave an asymptotic bubble speed that closely approximated the theoretical value.

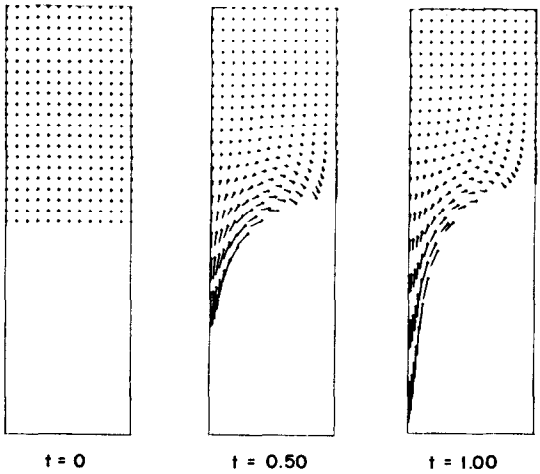

FIG. 9. Velocity plots for the Rayleigh-Taylor instability at times indicated.

The final example is the formation of a meniscus in a rectangular pipe with Bond number -4.0 and contact angle 60°. This calculation was performed with $\nu = 0.15$ and $\delta x = \delta y = 0.08$ with 25 cells in the horizontal direction and 6 in the vertical. The calculation begins with the horizontal surface at rest. Adhesion to the pipe wall at the left boundary immediately pulls the fluid upwards sending a wave to the right, Fig. 10. When the wave reflects from the symmetry plane at the right boundary (only the left half of the problem is shown in Fig. 10), a secondary swell is seen to form (fourth frame). The final frame shows the equilibrium meniscus. Actually, in this example the equilibrium configuration was artificially induced by setting all velocities to zero when the oscillating fluid surface was found to be close to the equilibrium position. The calculation was continued for 62 cycles after this zeroing to a time of $t = 4.0$ with negligible motion of the interface observed. This process greatly reduced the necessary computing time needed to reach equilibrium. A comparison between the equilibrium surface in Fig. 10 and the theoretical shape obtained by minimizing the potential energy of the system [14], agreed to within 0.1 per cent over the entire surface.

The Lagrangian zones have become significantly distorted near the left boundary at the time of the last frame in Fig. 10. However, this cell distortion does not significantly alter the equilibrium surface configuration. The wavelength of the disturbance is twice the mesh spacing, which gives a sawtooth appearance. There is little resistance to a sawtooth motion once it is excited. In this example, the sawtooth mode is excited when the top left corner vertex suddenly is pulled upwards by the wall adhesion. The distortion is seen to spread from the top left corner cell but is noticeably evident only in the last two frames. A study is currently underway of mechanisms that will damp this type of distortion.

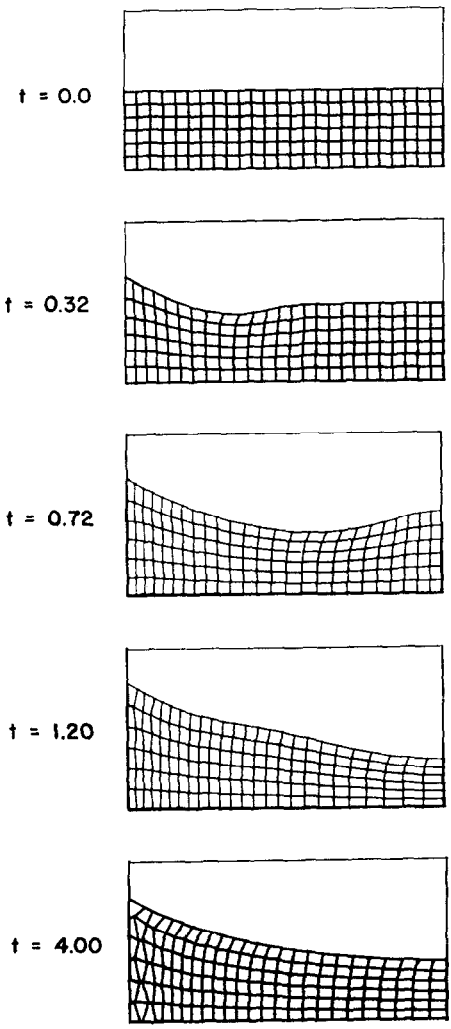

FIG. 10. Formation of a meniscus in a rectangular tank with Bond number −4.0. The fluid has reached its equilibrium configuration in the last frame.

G. CONCLUSION

A new method has been presented for calculating the transient dynamics of viscous incompressible fluids having free surfaces. The method uses Lagrangian coordinates, which makes the treatment of free surfaces and material interfaces

straightforward. The new method is illustrated by several test calculations that establish its validity and usefulness. In general, it is most suited for problems not undergoing large distortions, but requiring an accurate knowledge of free fluid boundaries. It is also useful for problems requiring high resolution in localized regions of the flow, such as a thin layer of fluid on the surface of another fluid.

APPENDIX

Detailed difference equations are written out in this appendix for two-dimensional Cartesian coordinates. The equations are for interior vertices and cells and do not reflect the special considerations needed at different types of boundaries, as described in Section C.

Vertices are moved with the advanced velocity values,

$$\left.\begin{aligned} {}^{n+1}x_i^j &= {}^{n}x_i^j + {}^{n+1}u_i^j\,\delta t, \\ {}^{n+1}y_i^j &= {}^{n}y_i^j + {}^{n+1}v_i^j\,\delta t. \end{aligned}\right\} \tag{A-1}$$

The velocities needed for vertex advancement are obtained from the following approximations used for the momentum equations,

$$\left.\begin{aligned} {}^{n+1}u_i^j &= {}^{n}u_i^j + \delta t[({}^{\phi}A_x)_i^j + ({}^{g}A_x)_i^j + ({}^{v}A_x)_i^j], \\ {}^{n+1}v_i^j &= {}^{n}v_i^j + \delta t[({}^{\phi}A_y)_i^j + ({}^{g}A_y)_i^j + ({}^{v}A_y)_i^j]. \end{aligned}\right\} \tag{A-2}$$

All quantities on the right side of (A-2) are evaluated at time step n. The various acceleration terms are

$$\begin{aligned} ({}^{\phi}A_x)_i^j = \frac{1}{2V_i^j}\,[&\phi_{i+1/2}^{j+1/2}(y_{i+1}^j - y_i^{j+1}) + \phi_{i-1/2}^{j+1/2}(y_i^{j+1} - y_{i-1}^j) \\ &+ \phi_{i-1/2}^{j-1/2}(y_{i-1}^j - y_i^{j-1}) + \phi_{i+1/2}^{j-1/2}(y_i^{j-1} - y_{i+1}^j)], \end{aligned}$$

$$\begin{aligned} ({}^{\phi}A_y)_i^i = \frac{1}{2V_i^j}\,[&\phi_{i+1/2}^{j+1/2}(x_i^{j+1} - x_{i+1}^j) + \phi_{i-1/2}^{j+1/2}(x_{i-1}^j - x_i^{j+1}) \\ &+ \phi_{i-1/2}^{j-1/2}(x_i^{j-1} - x_{i-1}^j) + \phi_{i+1/2}^{j-1/2}(x_{i+1}^j - x_i^{j-1})], \end{aligned}$$

$$\begin{aligned} ({}^{g}A_x)_i^j = \frac{g_x}{8V_i^j}\,[&(y_i^{j+1} - y_{i+1}^j)(x_{i+1}^{j+1} - x_i^j + x_{i+1}^j - x_i^{j+1}) \\ &+ (y_i^{j+1} - y_{i-1}^j)(x_i^{j+1} - x_{i-1}^j + x_i^j - x_{i-1}^{j+1}) \\ &+ (y_{i-1}^j - y_i^{j-1})(x_i^j - x_{i-1}^{j-1} + x_i^{j-1} - x_{i-1}^j) \\ &+ (y_{i+1}^j - y_i^{j-1})(x_{i+1}^j - x_i^{j-1} + x_{i+1}^{j-1} - x_i^j)], \end{aligned}$$

if index i is on a rigid vertical wall,

$$({}^{g}A_x)_i^j = g_x, \quad \text{otherwise,}$$

$$\begin{aligned}({}^{g}A_y)_i^j = \frac{g_y}{8V_i^j}\,[&(x_{i+1}^j - x_i^{j+1})(y_i^{j+1} - y_{i+1}^j + y_{i+1}^{j+1} - y_i^j)\\ &+ (x_i^{j+1} - x_{i-1}^j)(y_i^{j+1} - y_{i-1}^j + y_{i-1}^{j+1} - y_i^j)\\ &+ (x_i^{j-1} - x_{i-1}^j)(y_{i-1}^j - y_i^{j-1} + y_i^j - y_{i-1}^{j-1})\\ &+ (x_{i+1}^j - x_i^{j-1})(y_{i+1}^j - y_i^{j-1} + y_i^j - y_{i+1}^{j-1})],\end{aligned}$$

if index j is on a rigid horizontal wall,

$$({}^{g}A_y)_j^i = g_y, \quad \text{otherwise,}$$

$$\begin{aligned}({}^{\nu}A_x)_i^j = \frac{\nu}{2V_i^j}\,[&\omega_{i+1/2}^{j+1/2}(x_i^{j+1} - x_{i+1}^j) + \omega_{i-1/2}^{j+1/2}(x_{i-1}^j - x_i^{j+1})\\ &+ \omega_{i-1/2}^{j-1/2}(x_i^{j-1} - x_{i-1}^j) + \omega_{i+1/2}^{j-1/2}(x_{i+1}^j - x_i^{j-1})],\end{aligned}$$

$$\begin{aligned}({}^{\nu}A_y)_i^j = \frac{\nu}{2V_i^j}\,[&\omega_{i+1/2}^{j+1/2}(y_i^{j+1} - y_{i+1}^j) + \omega_{i-1/2}^{j+1/2}(y_{i-1}^j - y_i^{j+1})\\ &+ \omega_{i-1/2}^{j-1/2}(y_i^{j-1} - y_{i-1}^j) + \omega_{i+1/2}^{j-1/2}(y_{i+1}^j - y_i^{j-1})].\end{aligned}$$

In the last two accelerations we have introduced a cell vorticity, which is defined as

$$\begin{aligned}\omega_{i+1/2}^{j+1/2} = \frac{1}{2V_{i+1/2}^{j+1/2}}\,[&(v_i^{j+1} - v_{i+1}^j)(y_i^j - y_{i+1}^{j+1}) - (v_{i+1}^{j+1} - v_i^j)(y_{i+1}^j - y_i^{j+1})\\ &+ (u_i^{j+1} - u_{i+1}^j)(x_i^j - x_{i+1}^{j+1}) - (u_{i+1}^{j+1} - u_i^j)(x_{i+1}^j - x_i^{j+1})].\end{aligned} \tag{A-3}$$

The factor of 1/2 in ${}^{\phi}A$ and ${}^{\nu}A$ arises because the integration volumes used to calculate these average accelerations are twice as big as the volume of the vertex. Recall that a vertex volume is 1/4 the sum of the quadrilateral volumes touching the vertex,

$$V_i^j = 1/4(V_{i+1/2}^{j+1/2} + V_{i-1/2}^{j+1/2} + V_{i-1/2}^{j-1/2} + V_{i+1/2}^{j-1/2}). \tag{A-4}$$

The gravitational accelerations are not simply g_x and g_y, but have dimensionless ratios multiplying them. These ratios are necessary to simplify the free-slip boundary conditions at a rigid wall.

To conserve volume the pressures needed in (A-2) must satisfy the equation derived by substituting the new velocities (A-2) into the volume equations

$${}^{n+1}V_{i+1/2}^{j+1/2} = {}^{0}V_{i+1/2}^{j+1/2},$$

which produces (12). Rewriting (12) so the pressures appear explicitly we have

$$\beta\phi_{i+1/2}^{j+1/2} = -[\gamma_R\phi_{i+3/2}^{j+1/2} + \gamma_{UR}\phi_{i+3/2}^{j+3/2} + \gamma_U\phi_{i+1/2}^{j+3/2} + \gamma_{UL}\phi_{i-1/2}^{j+3/2} + \gamma_L\phi_{i-1/2}^{j+1/2} + \gamma_{BL}\phi_{i-1/2}^{j-1/2} + \gamma_B\phi_{i+1/2}^{j-1/2} + \gamma_{BR}\phi_{i+3/2}^{j-1/2}] + R_{i+1/2}^{j+1/2}. \tag{A-5}$$

The γ factors and β for cell $i + 1/2$, $j + 1/2$ are defined as

$$\beta = \frac{1}{V_i^j}[(x_i^{j+1} - x_{i+1}^j)^2 + (y_i^{j+1} - y_{i+1}^j)^2] + \frac{1}{V_{i+1}^j}[(x_i^j - x_{i+1}^{j+1})^2 + (y_i^j - y_{i+1}^{j+1})^2] + \frac{1}{V_{i+1}^{j+1}}[(x_{i+1}^j - x_i^{j+1})^2 + (y_{i+1}^j - y_i^{j+1})^2] + \frac{1}{V_i^{j+1}}[(x_{i+1}^{j+1} - x_i^j)^2 + (y_{i+1}^{j+1} - y_i^j)^2],$$

$$\gamma_R = \frac{1}{V_{i+1}^j}[(x_i^j - x_{j+1}^{i+1})(x_{i+1}^{j+1} - x_{i+2}^j) + (y_i^j - y_{i+1}^{j+1})(y_{i+1}^{j+1} - y_{i+2}^j)] + \frac{1}{V_{i+1}^{j+1}}[(x_{i+1}^j - x_i^{j+1})(x_{i+2}^{j+1} - x_{i+1}^j) + (y_{i+1}^j - y_i^{j+1})(y_{i+2}^{j+1} - y_{i+1}^j)],$$

$$\gamma_{UR} = \frac{1}{V_{i+1}^{j+1}}[(x_{i+1}^j - x_i^{j+1})(x_{i+1}^{j+2} - x_{i+2}^{j+1}) + (y_{i+1}^j - y_i^{j+1})(y_{i+1}^{j+2} - y_{i+2}^{j+1})],$$

$$\gamma_U = \frac{1}{V_{i+1}^{j+1}}[(x_{i+1}^j - x_i^{j+1})(x_i^{j+1} - x_{i+1}^{j+2}) + (y_{i+1}^j - y_i^{j+1})(y_i^{j+1} - y_{i+1}^{j+2})] + \frac{1}{V_i^{j+1}}[(x_{i+1}^{j+1} - x_i^j)(x_i^{j+2} - x_{i+1}^{j+1}) + (y_{i+1}^{j+1} - y_i^j)(y_i^{j+2} - y_{i+1}^{j+1})],$$

$$\gamma_{UL} = \frac{1}{V_i^{j+1}}[(x_{i+1}^{j+1} - x_i^j)(x_{i-1}^{j+1} - x_i^{j+2}) + (y_{i+1}^{j+1} - y_i^j)(y_{i-1}^{j+1} - y_i^{j+2})],$$

$$\gamma_L = \frac{1}{V_i^j}[(x_i^{j+1} - x_{i+1}^j)(x_{i-1}^j - x_i^{j+1}) + (y_i^{j+1} - y_{i+1}^j)(y_{i-1}^j - y_i^{j+1})] + \frac{1}{V_i^{j+1}}[(x_{i+1}^{j+1} - x_i^j)(x_i^j - x_{i-1}^{j+1}) + (y_{i+1}^{j+1} - y_i^j)(y_i^j - y_{i-1}^{j+1})],$$

$$\gamma_{BL} = \frac{1}{V_i^j}[(x_i^{j+1} - x_{i+1}^j)(x_i^{j-1} - x_{i-1}^j) + (y_i^{j+1} - y_{i+1}^j)(y_i^{j-1} - y_{i-1}^j)],$$

$$\gamma_B = \frac{1}{V_i^j}[(x_i^{j+1} - x_{i+1}^j)(x_{i+1}^j - x_i^{j-1}) + (y_i^{j+1} - y_{i+1}^j)(y_{i+1}^j - y_i^{j-1}) + \frac{1}{V_{i+1}^j}[(x_i^j - x_{i+1}^{j+1})(x_{i+1}^{j-1} - x_i^j) + (y_i^j - y_{i+1}^{j+1})(y_{i+1}^{j-1} - y_i^j)],$$

$$\gamma_{BR} = \frac{1}{V_{i+1}^j}[(x_i^j - x_{i+1}^{j+1})(x_{i+2}^j - x_{i+1}^{j-1}) + (y_i^j - y_{i+1}^{j+1})(y_{i+2}^j - y_{i+1}^{j-1})].$$

The source term in (A-5) is

$$R_{i+1/2}^{j+1/2} = -4\left\{\frac{1}{\delta t^2}\left({}^{n}V_{i+1/2}^{j+1/2} - {}^{0}V_{i+1/2}^{j+1/2}\right) + \frac{1}{\delta t}\sum_{k,l} a_{kl}(u_l y_k + x_l v_k)\right.$$
$$+ \sum_{k,l} a_{kl} u_l v_k + \sum_{k,l} a_{kl}[({}^{u}A_x)_l\, y_k + x_l({}^{u}A_y)_k]$$
$$\left. + \sum_{k,l} a_{kl}[({}^{v}A_x)_l\, y_k + x_l({}^{v}A_y)_k]\right\},$$

where summations are over cell vertices as in the definition of a_{kl} in (11). Equation (A-5) is a Poisson equation for the pressure that is solved using a Gauss-Seidel iteration with successive-over-relaxation. Once the pressures are determined from (A-5), with the appropriate boundary conditions, they can be used to calculate new u and v values, using (A-2). Because of the way the pressure equation was derived, when the vertices are moved according to (A-1) the new cell volumes remain unchanged.

Acknowledgment

We would like to express our appreciation to Francis H. Harlow and Richard A. Gentry for many interesting discussions.

References

1. J. E. Fromm, Los Alamos Scientific Laboratory Report LA-2910 (1963); J. E. Fromm and F. H. Harlow, *Phys. Fluids* **6**, 975 (1963); C. E. Pearson, *Jour. Fluid Mechanics* **21**, 611 (1965); D. C. Thoman and A. A. Szewczyk, Heat Transfer and Fluid Mechanics Laboratory, Dept. of Mechanical Engineering, University of Notre Dame, Technical Report 66-14 (1966).
2. F. H. Harlow and J. E. Welch, *Phys. Fluids* **8**, 2182 (1965); F. H. Harlow, J. E. Welch, J. P. Shannon, and B. J. Daly, Los Alamos Scientific Laboratory Report LA-3425 (1965); A. J. Chorin, *J. Comp. Phys.* **2**, 12 (1967).
3. K. Aziz and J. D. Hellums, *Phys. Fluids* **10**, 314 (1967); J. E. Fromm, Los Alamos Scientific Laboratory Report LA-3522.
4. C. W. Hirt and F. H. Harlow, *J. Comp. Phys.* **2**, 114 (1967).
5. B. J. Daly, to be published in *J. Comp. Phys.* **4**, 97 (1969).
6. F. H. Harlow, J. E. Welch, J. P. Shannon, and B. J. Daly, Los Alamos Scientific Laboratory Report LA-3425, Part 4, (1965).
7. C. W. Hirt and J. P. Shannon, *J. Comp. Phys.* **2**, 403 (1968).
8. J. E. Fromm, Los Alamos Scientific Laboratory Report LA-2535 (1961).
9. C. W. Hirt, *J. Comp. Phys.* **2**, 339 (1968).
10. F. H. Harlow and J. E. Welch, *Phys. Fluids* **9**, 842 (1966).
11. R. Chan, Thesis submitted to the Dept. of Civil Engineering, Stanford University (1969).
12. I. Tadjbakhsh and J. B. Keller, *J. Fluid Mech.* **8**, 442 (1960).
13. P. R. Garabedian, *Proc. Roy. Soc. (London)* **A241**, 423 (1957).
14. P. Concus, *Advan. Astronautical Sci.* **14**, 21 (1963).